Pressure broadening of 772.376 and 772.421 nm argon lines and kinetics of argon metastable atoms

Nader Sadeghi, Romain Magnan, Françoise Massines

Pressure broadening of 772.376 and 772.421 nm argon lines and kinetics of argon metastable atoms

Nader Sadeghi[1,*], Romain Magnan[2] and Françoise Massines[2]

[1,] Laboratoire Interdisciplinaire de Physique (LIPhy CNRS, UMR 5588) & Laboratoire des Technologies de la Microélectronique (LTM, CNRS, UMR 5129), Université de Grenoble-Alpes, Grenoble, France

[2] Laboratoire Procédés Matériaux et Énergie Solaire (PROMES, CNRS, UPR 8521), Rambla de la thermodynamique, 66100 Perpignan, France

Abstract

Tunable diode laser absorption spectroscopy is used for recording the spectrally mixed profiles of argon 772.376 nm ($2p_7$-$1s_5$) and 772.421 nm ($2p_2$-$1s_3$) lines at different argon background pressures between 0.3 and 1 atmosphere. The absorbing atoms in the Ar*($1s_5$) and Ar*($1s_3$) metastable states are produced in a plane-to-plane dielectric barrier glow discharge operating at 20 kHz. The pressure broadening coefficient *w* and wavelength shift, *s* of the lines, deduced from the analysis of their variation versus pressure of recorded profiles, are w_1=28.3±2.0 pm (14.2±1.0 GHz) and s_1=11.5±0.8 pm (-5.8±0.4 GHz) for 772.376 nm line and w_2=36.3±0.5 pm (18.2±0.3 GHz) and s_2=12.8±0.7 pm (-6.4±0.4 GHz) for 772.4207 nm line, at 1 bar and 300 K. The progressive enhancement with argon pressure of the peak densities ratio [Ar*($1s_3$)]/[Ar*($1s_5$)], reaching 0.3 at 1 bar, reveals the importance of Ar-induced collisions for the population transfer from resonant $1s_2$ to the metastable $1s_3$ state. Also, the time variation of Ar*(1s) densities indicates the presence of a weak excitation channel outside the discharge current pulse initiated by the breakdown. This channel results from the heating of electrons by the electric field seen by the gas in the DBD gap.

Keywords: Argon 772 nm lines, Pressure broadening, Pressure shift, Tunable diode laser absorption spectroscopy, Dielectric barrier discharges, Collision, Population transfer.

* Corresponding author; E-mail: nader.sadeghi@univ-grenoble-alpes.fr

1. Introduction

In the last decades, atmospheric pressure non-equilibrium room temperature plasmas (APRTP) attracted high attention due to their particular physical properties. Thanks to the presence of high energy electrons, these plasmas can dissociate stable molecules to produce highly reactive radicals, or provide large density of atoms and molecules in highly excited electronic states, in an environment with heavy particles remained close to the room temperature. These properties have stimulated their application to "local" treatment of heat-sensitive surfaces in medicine[1, 2], sterilization[3, 4, 5], material processing[6] and in many other domains (see also review papers [7, 8, 9, 10, 11] and references therein). In most of APRTPs, helium or argon is used as main plasma-generating gas and their metastable atoms play an important role in plasma chemical processes. These atoms can be the main factor of the plasma sustainment through Penning and chemi-ionization of the trace or admixture molecules[12]. They also can highly influence the production rate of reactive radicals through e-ion recombination of so produced molecular ions[13, 14]. When modeling APRTPs, the knowledge of the gas temperature, T_g is of prime importance because most of the reaction coefficients of species present are T_g dependent[13,14,15, 16]. One way to determine the gas temperature would be from the rotational temperature of a molecule present in the plasma as impurity[17, 18], but this technique cannot be used in high purity rare-gases. Another technique, currently applied in low pressure rare gas plasmas, is the use of an appropriate tunable diode laser for deducing T_g from the Doppler width of the Gaussian profile of a spectral line whose lower level is a metastable state of the rare-gas [19, 20, 21]. But in APRTPs, collision of the excited -emitter or absorber- atom with ground-state atoms induces the spectral broadening of the line (pressure broadening), which evidences by the presence of a Lorentzian component in their line profile. When the upper or lower level of the considered atomic transition is optically connected to the ground state of the collision partner, the interaction is dominantly dipole-dipole type, leading to "resonance broadening" with T_g^{-1} gas temperature dependence[22]. Otherwise, it is dipole-induced-dipole interaction, leading to the "Van der Waals broadening", whose temperature dependence is $T_g^{-0.7}$ [22]. Therefore, the knowledge of the pressure broadening coefficient of the line would permit the determination of the gas temperature from its recorded profile[23] .

In 1960-1970s, motivated by the determination of the oscillator strength of resonance lines of rare-gas atoms, but also for testing the applicability of different collision broadening theories, several groups have measured the pressure broadening coefficients of different argon

lines. The resonance Faraday effect on some argon lines absorbed by metastable atoms has been used in [24, 25], but most of the line profiles were obtained from the analysis of the profile of plasma induced emission, by scanning Fabry-Perot interferometer[26, 27, 28] or with a spectrometer[29, 30, 31, 32]. However, the necessary correction for the apparatus function of the experimentally recorded spectral profiles of the lines introduced large uncertainty on deduced broadening coefficients. Moreover, often in thermal plasmas the gas temperature was not homogeneous and well defined [29, 28, 32], introducing extra uncertainty on measured coefficients. But after the event of the spectrally narrow band tunable diode lasers and their use in absorption spectroscopy (TDLAS) technique, the correction of the apparatus function width was no more needed and the pressure induced widths and shifts of many argon lines ending on the four lowest excited states of argon (two metastable Ar*($1s_3$) and Ar*($1s_5$) and two resonant Ar*($1s_2$) and Ar*($1s_4$)[33]), which are always highly populated in argon plasmas, have been measured by several groups[34, 35, 36, 37, 38, 39, 40]. Also, Nayak *et al* have recently applied the broad-band absorption spectroscopy technique for measuring the pressure broadening coefficients of 750.39, 751.47, 763.51 and 794.82 nm argon lines[41]. However, none of the above cited publications provided the pressure broadening coefficients of the 772.38 nm ($1s_5$-$2p_7$) and 772.42 nm ($1s_3$-$2p_2$) lines, which are studied in this work.

In this work, the absorption profiles of the combined 772 nm lines are measured in low energy glow type dielectric barrier discharges (DBD) for Ar pressures between 0.3 and 1 atmosphere. From these measurements, the pressure broadening coefficients and wavelength shifts of the 772.376 and 772.4207 nm lines are deduced. Also, the variation of the [Ar*($1s_3$)]/[Ar*($1s_5$)] density ratio versus the Ar pressure is pointed out and the kinetics of Ar*(1s) atoms in the pulse DBD is explained.

2. Experimental setup

Metastable atoms in Ar*($1s_3$) and Ar*($1s_5$) states, the lower levels of the studied transitions, are produced by dielectric barrier discharge (DBD) in pre-mixed Ar + 200 ppm of NH_3 Penning gas. The metallic electrodes of the plane-to-plane DBD are covered by 1 mm-thick, 70 mm x 70 mm dielectric plates made of alumina, with 2 mm gap between them. The discharge zone is 50 x 10 x 2 mm^3 volume, defined by the dimensions of electrodes. The whole DBD cell is contained in an air-tighten chamber. Before each experiment, the chamber is pumped down to 10 µbar and, to reduce the amount of impurity resulting from eventual air leak and degassing from walls, it is then flushed with 3 standard liters per minute (SLM) of

the gas mixture. A needle valve between the chamber and the pumping pipe permits to adjust the total pressure in the chamber, measured with a capacitance gauge, between 0.3 and 1 bar. Considering the 5 x 0.2 cm^2 section of the gas flow, the 3 slm flow rate and μ=2.2 $x10^{-5}$ $Kg.m^{-1}.s^{-1}$ dynamic viscosity of argon, Reynolds number is smaller than 300 for all considered pressures, resulting in a laminar gas flow between dielectric plates. The top electrode of the DBD is powered by a 20 kHz generator (Keysight 33500B Series) followed by an audio amplifier (Crest CC4000) and voltage transformer (Boige & Vignal), while the bottom electrode is grounded. Depending on the pressure fixed in the chamber, the amplitude of the applied high voltage (HV) is adjusted (up to 2000 V peak value) for obtaining stable and reproducible discharges, but at the lowest possible voltage to limit the electron density. Current-voltage characteristics are obtained using a high-voltage probe (Tektronix P6015A 75 MHz) and a current probe (LILCO LTD 13W5000), whose signals are recorded and processed on an oscilloscope (Tektronix MSO56). Figure 1 shows three V-I curves, over one period of the HV, for three pressures. The discharge current is characteristic of a glow DBD, free of microdischarges[42]. As the discharge covers uniformly all the DBD volume between electrodes, the discharge current was deduced by subtracting the displacement current (recorded at the same voltage but in an empty chamber) from the total current and the voltage applied to the gas gap V_g, was calculated by accounting for the charges deposited on the surface of dielectrics from the previous discharge[43]. As seen from this figure, higher the pressure, larger the applied voltage amplitude is. But in all cases, the peak discharge current remains about 20 mA (40 $A.m^{-2}$ current density). Deduced from the V-I curves, for all studied pressures the dissipated power in the gas remains below 0.1 mJ per discharge pulse. The calculated gas drift velocity at 1 atmosphere is 0.5 m/s, corresponding to a residence time inside the discharge volume of 20 ms. Thus, the deposited power on the gas during the residence time of the gas is <40 mJ. Most of this energy is transferred to dielectric electrodes; both by heat conduction and by ion accelerated within the sheaths (see Ref 44 for more detail). The gas temperature deduced from the Gaussian component of the Voigt profile fitting the absorption lines at 312 mbar (see section 3.) is about 310 K. This very small increase of the gas temperature by the plasma action was also confirmed by the spectral simulation of the plasma induced emission intensity of the nitrogen first positive 4-1 band, at 678 nm, from atmospheric pressure argon + 0.04% N_2 DBD (see Figure 2). Fitting parameter for the temperature was 305 ±10 K. Thus, at all pressures, the width of the Gaussian component of the Voigt functions fitting the experimental line profiles (see section 3) was fixed to w_G (FWHM)= 0.774 GHz = 1.54 pm= 0.706 step, corresponding to a gas temperature of 310 K.

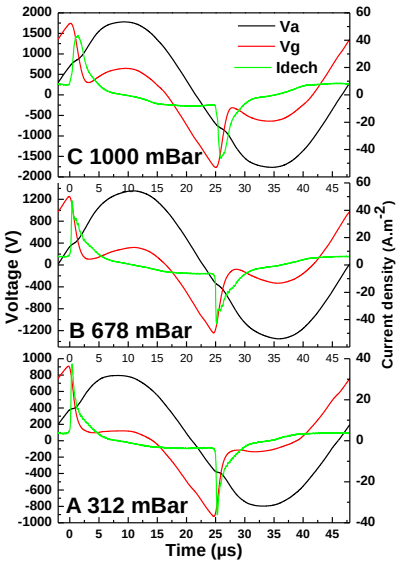

Figure 1. V-I characteristics of the DBD discharge at three pressures inside the chamber. The current density, Idech is deduced by subtracting the displacement current from the total current and V_a and V_g are the voltage applied to electrodes and in the gas gap, respectively.

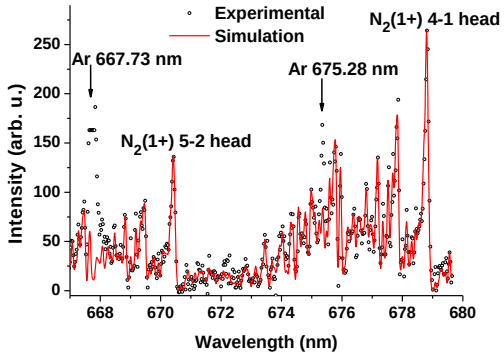

Figure 2. Experimental (circle) and simulated spectra with T_g=305 K (solid line) of (4→1) and (5→2) bands of the 1st positive system of nitrogen with 0.04% N_2 added to atmospheric pressure argon DBD plasma. Arrows show the argon 667.73 nm (fully saturated) and 675.28 nm lines positions.

3. Recording absorption line profiles

The spectral profile of the combined 772 nm lines is recorded by tunable laser absorption spectroscopy (TDLAS) technique[35, 21] on argon metastable atoms produced mainly during current pulses. A distributed feedback diode laser (DFB, DL100, Toptica) (DL), working around 772 nm is used. Its scan over few hundreds of GHz (a few 0.1 nm) is obtained by changing the temperature of the DL. In this wavelength range, atoms in the most

populated Ar*($1s_5$) metastable state[33] can absorb the laser light on $1s_5$-$2p_7$ transition at 772.3761 nm and atoms in the other metastable Ar*($1s_3$) state absorb the laser light on $1s_3$-$2p_2$ transition at 772.4207 nm[45]. But given the closeness of these two transitions and the respective pressure broadening of the lines, their profiles are gradually mixed up with increasing argon pressure. The sketch of the optical set-up for the TDLAS measurements is shown in figure 3. The laser beam from the DL passes through a beam-splitter (BS) which provides two secondary beams. One of them goes through a low-pressure argon discharge reference cell (RC) and is detected with a silicon photodiode (PD1). The other secondary beam crosses a 20 cm long confocal Fabry-Perot interferometer (FPI) and is detected by PD2. The mode-hop-free functioning and the linear frequency change of the DL versus its temperature, are controlled from the regularity of the transmitted peak of the FPI. The absorption signal from the low-pressure Ar discharge cell permits to localize the non-shifted central wavelength, λ_0 of the lines. The main laser beam goes through the DBD device and is detected by a fast silicon photodiode, backed with a trans-impedance amplifier PD3 (New Focus 1801, 125 MHz bandwidth and G=40V/mA), which provides 3 ns temporal resolution. A diaphragm limits the laser beam diameter to about 1 mm inside the DBD and appropriate optical attenuators on the path of the beams reduce the laser intensities to avoid optical saturation in the DBD and in the low- pressure argon cell plasma. Signals from all three PDs are recorded with a 400 MHz bandwidth digital oscilloscope (Lecroy 44Xi) triggered in phase with the HV waveform, averaged over 2000 cycles of the HV and hence stored for the data processing. 1001 data points, with a time interval of 50 ns are taken during the 50 µs period of the HV. Thus the final time resolution of the records is 50 ns.

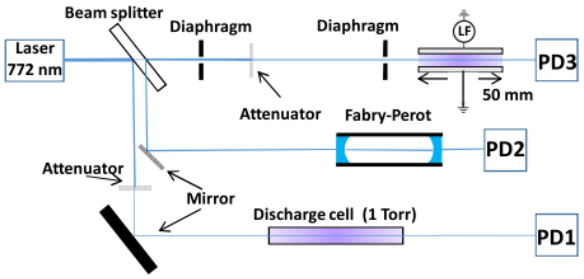

Figure 3. Experimental setup used for determination of Ar metastable atoms densities by absorption spectroscopy using a tunable diode laser. PDs represent photodiodes.

As already pointed out, metastables atoms in the DBD are mainly produced during the current pulses, whose duration is about 1-2 µs. Considering the about 1 µs lifetime of Ar*

metastable atoms at the studied pressure range (0.3-1 bar)[44], their densities evolve along the 50 µs period of the high voltage. It is thus not possible to obtain the absorption profiles by the direct continuous scan of the laser frequency, as is usually done in non time-varying plasmas, by the current scan of the DL[46, 47, 48]. The method we use consists in recording the time-varying transmitted laser signal (TVTLS) at various fixed laser wavelengths and using these records for obtaining the absorption profiles at different times of the HV period. For each argon pressure, about 50 TVTLS have been recorded in the 772.35 to 772.47 nm interval by changing the temperature of the diode laser by fixed steps of about 5 mK. Calibrated from the 375.0 MHz free spectral range (FSR) of the FPI and the precise 44.66 pm wavelength gap between the two studied argon lines[45], the precise wavelength interval between the successive acquisition steps is $\delta\lambda$=2.180±0.025 pm (corresponding to $\delta\nu$=1.096±0.013 GHz). In figure 4 are reported some of the recorded signals from PD3 for 312 mbar argon pressure. The origin of the time is the same as in Fig. 1 and corresponds to the start of the fast discharge current increase in the positive half-period of the HV and signals after t=25 µs are relative to the 2nd discharge pulse on the negative half-period of the HV. Only the time-varying parts of the recorded data are shown in this figure. Emission signal from the DBD plasma, E(t) is also shown in the bottom of the figure and its amplitude before the start of the discharge pulse (t<0) is the offset of the detector, the background (BG). Plasma emission pulses are in accordance with the discharge current pulses.

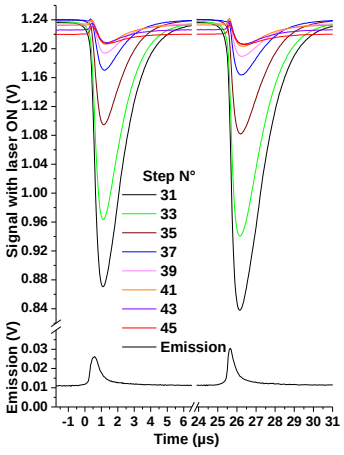

Figure 4. Signals from PD3 during the most significant parts of one HV period at Ar pressure of 312 mbar. Note breaks on both time and amplitude axis and different scales for the emission (laser blocked) and laser ON signals. Step 31 is when the laser wavelength is at the maximum absorption of the 772.42 nm line and the following steps are with the laser

shifted in its red wing. Each step corresponds to 2.18 pm. For the sake of clarity, only records with odd step numbers are plotted.

The signal $S_n(\lambda_n, t)$ of PD3, when the laser is set at the wavelength λ_n of step number n, corresponds to the sum of the transmitted laser light, $I_n(\lambda_n, t)$ plus the plasma emission E(t). Thus, the time-varying plasma transmitted laser intensity can be deduced as $I_n(\lambda_n, t)=S_n(\lambda_n, t)-E(t)$. The transmitted laser intensity before the start of the discharge pulse $I_{0n}(\lambda_n)$ at t<0, thus in the absence of metastable atoms, provides the absorption-free laser intensity for the step N° n. Note the slight variation of the laser intensity with the wavelength, which should be related to the temperature variation of the DL, which is scanned by changing its temperature. For each step, thus λ_n value, the Beer-Lambert law relates the time-varying absorbance $\mathcal{A}_n(\lambda_n, t)$ to the absorbing atoms densities, N(t):

$$\mathcal{A}_n(\lambda_n, t) = \mathrm{Ln}\left(\frac{I_{0n}(\lambda_n)}{I_n(\lambda_n,t)}\right) = \left(k_5.N_5(t).\varphi_5(\lambda_n) + k_3.N_3(t).\varphi_3(\lambda_n)\right).L \qquad (1)$$

where the subscripts 5 and 3 refer to metastable atoms in $Ar(1s_5)$ and $Ar(1s_3)$ states, with their respective densities $N_5(t)$ and $N_3(t)$ at time *t* in the HV cycle, L=5 cm is the absorption length in the DBD and *k*(m^3) is the line dependent absorption coefficient, defined as[41, 49]:

$$k = \frac{g_u}{g_l}.\lambda_0^4.\frac{A_{ul}}{8\pi c} \qquad (2)$$

in which g_u and g_l refer to the statistical weights of the upper and lower levels of the transition at wavelength λ_0 with Einstein coefficient A_{ul}. $\varphi_5(\lambda_n)$ and $\varphi_3(\lambda_n)$ in Eq.(1) are normalized profiles of the 772.38 and 772.42 nm lines, defined as $\int \varphi(\lambda).d\lambda = 1$.

A matrix is built, with $\mathcal{A}_n(\lambda_n, t)$ files forming its columns and the time in the HV period being its rows. Once transposed, the successive columns of the new matrix provide the absorption profiles at different times of the HV period. As an example, two reconstructed absorption profiles from absorbance measurements in the 455 mbar DBD plasma are presented in figure 5. Profile in 5A corresponds to the time of the peak absorbance in the positive half-period of the HV. This time is at about 1 µs after the start of the discharge current. And the profile in 5B is in the afterglow, about 2.75 µs later than for 5A. The about 0.7 µs delay of the peak metastable density relative to the peak of the plasma induced emission, which corresponds to the peak of the discharge current in the DBD, results from the

about 1 µs lifetime of Ar* metastable atoms. This delay also exists for all other pressures and is clearly seen in Fig. (4) for the 312 mbar plasma.

The reconstructed absorption profile is fitted with the sum of two Voigt functions, $V_5(\lambda)$ and $V_3(\lambda)$ (dashed blue and red curves in Fig. 5, respectively). They represent the pressure broadened absorption profiles of 772.38 nm Ar($1s_5$-$2p_7$) and 772.42 nm Ar($1s_3$-$2p_2$) lines, respectively. Their amplitudes inform us about the density of metastable atoms at different times for the considered pressure. The pressure broadening coefficients of the lines and the gas temperature can be deduced from the Lorentzian and Gaussian widths of the Voigt profiles. At fixed pressures, two sets of absorption measurements have been acquired and the concordance between the parameters of the reconstructed profiles from them has been verified. We have also observe that at given pressure, the width of the fitting Voigt functions remained unchanged (within 5%) whatever the discharge pulse position (positive or negative half-period of the HV) or the time in the period for which the absorption profile was reconstructed. This indicates a non-varying gas temperature during the LF period.

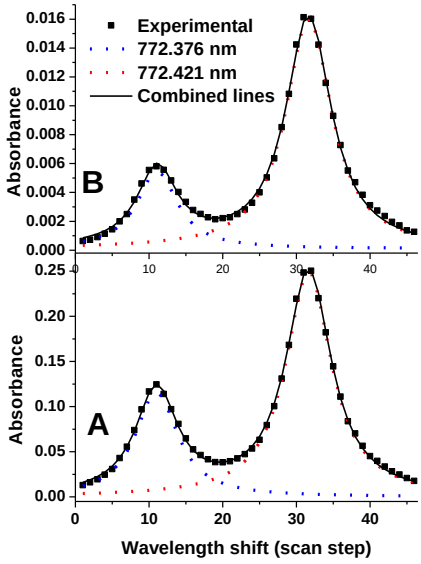

Figure 5. Reconstructed absorption profiles at the peak absorbance (A) and 2.75 µs later (B) in 455 mbar DBD plasma, presented with the Voigt profile fits of 772.376 (dashed blue) and 772.421 (dashed red) nm lines. The wavelength step of the DL scan is $\delta\lambda$=2.18 pm.

4. Pressure broadening and shift coefficients of lines

Reconstructed absorption profiles of the combined 772.376 nm and 772.4207 nm lines for the five studied argon pressures in the DBD chamber between 312 and 1000 mbar are presented in figure 6. Given the less than 10 MHz spectral width of the laser and its better than 100 MHz stability, tested over an hour by recording the amplitude of the transmitted peak of the Fabry-Perot interferometer, the apparatus function can be considered as negligible. Thus, profiles shown in Fig. 6 are the exact absorption profiles of the lines at corresponding pressures. The red vertical lines indicate the non-shifted positions of these lines, obtained from the peak absorptions in the low-pressure argon discharge cell. For each pressure, the black solid curve represents the best fitting to the experimental absorption profile with the sum of two Voigt functions, which are presented as blue and red solid curves for 772.376 and 772.4207 nm lines, respectively. To obtain the lowest noise level on reconstructed line profiles, those shown in Fig. 6 have been obtained at the peak absorbance, reached at the maxima metastable atoms densities. Also, the path of the laser beam in the gap of the DBD has been selected for having the largest absorbance. For pressures less than 0.5 bar, the laser beam crossed the DBD in the middle of the gap between electrodes but it was slightly shifted toward one of the electrodes at higher pressures. However, due to the quenching of metastable atoms by 3-body collisions with two ground state Ar atoms[44, 50], the density of metastable atoms continuously decreases with increasing pressure.

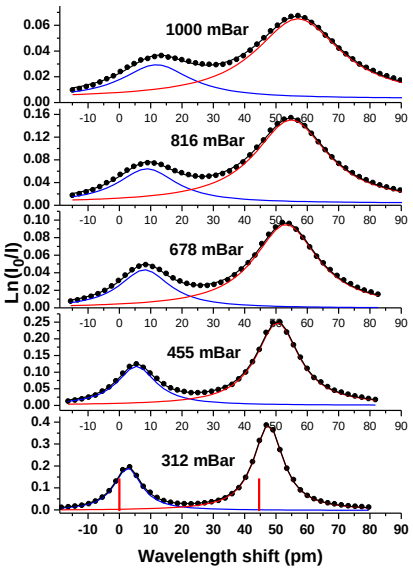

Figure 6. Reconstructed absorption profiles at five argon pressures between 312 and 1000 mbar. The wavelengths' origin is the non-shifted spectral position (at low pressure) of

the 772.376 nm line, indicated by a red vertical line at 0. The red vertical line at 44.7 pm indicates the non-shifted position of the 772.4207 nm line.

The enhancement of the line-widths with increasing pressure is clearly evidenced in Fig. 6. 772.376 nm and 772.4207 nm lines, which are almost separated at 312 mbar, become completely mixed at atmospheric pressure. The shift of their central wavelengths relative to their respective zero pressure positions also increases with argon pressure. In DBD plasmas, the electron density barely exceeds 10^{18} m^{-3} [44], for which the reported Stark width of the lines would be 0.0007 and 0.0008 pm, respectively[51]. The Stark broadening of the lines can thus be neglected and the Lorentzian components of the Voigt functions fitting their profiles represent their pressure broadened widths. Figure 7 shows for both lines the pressure dependence of the full width at half maximum (FWHM) and shift (s) of their Lorentzian components. As expected from the theory, which will be discussed later, the pressure dependence is linear and the solid lines, which are the best linear fit to the experimental data (in black for the 772.4207 nm and in red for the 772.376 nm lines), have been forced to start from the origin of the pressure and of the ordinates in each case. The full width at half maximum (w) and shift (s) of these lines, deduced from their respective slops are: w_1=27.7±2 pm.bar^{-1} and s_1=11.3±0.8 pm.bar^{-1} for 772.376 nm line and w_2=35.5±0.5 pm.bar^{-1} and s_2=12.5±0.7 pm.bar^{-1} for 772.421 nm line. Reported uncertainties correspond to 2σ of the fit +1.3% uncertainty from the wavelength gap between steps. However, given the estimated gas temperature of 310 K and the $T^{-0.7}$ dependence of both width and shift parameters (see section 4.1), the broadening and shift values at standard conditions of atmospheric pressure and 300 K would be w_1=28.3±2 pm and s_1=11.5±0.8 pm for 772.376 nm line and w_2=36.3±0.5 pm and s_2=12.8±0.7 pm. In section 6.1, these values will be compared to available experimental data and theory prediction.

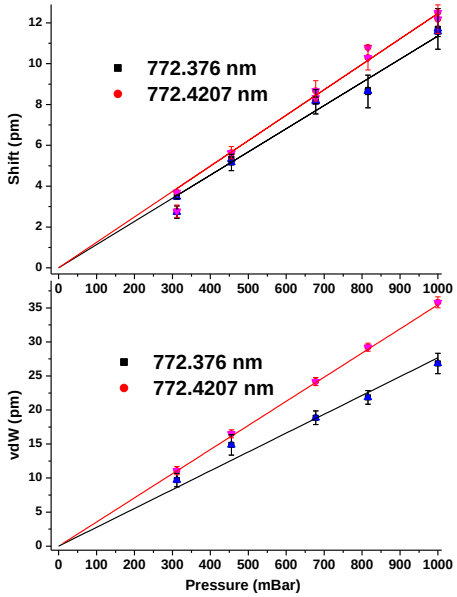

Figure 7. Pressure dependence of the respective Lorentzian widths (FWHM) and shifts of studied lines, deduced from fitting of their absorption profiles with Voigt functions.

4.1. Theoretical broadening coefficient of lines

None of the lower or upper levels of the studied lines are optically connected to the ground state. Therefore, the broadening comes from the Van der Waals interaction of excited atoms with surrounding argon atoms. The FWHM of the Van der Waals broadening, $\Delta\lambda_{vdW}$ is expressed as[52]:

$$\frac{\Delta\lambda_{vdW}}{[Ar]} \cong 3.0\,x10^{-15}.\lambda^2.(C_{6u}-C_{6l})^{2/5}.(T_g/\mu)^{3/10} \qquad (3)$$

where [Ar] is the argon density (in cm^{-3}), λ the wavelength and $\Delta\lambda_{vdW}$ are in nm, μ=20 is the reduced mass of collision partners in atomic unit and T_g is the gas temperature. C_{6u} and C_{6l} are Van der Waals coefficients of upper and lower levels of the transition, expressed as:

C_6=9.8 x $10^{-10}\alpha_p R^2$, in which the polarizability of the ground state argon is[53] α_p =1.64 10^{-24} cm^3 and R^2 (in unit of Bohr radius a_0) is a parameter defined as[25]:

$$R_i^2 = \left(\frac{5}{2}\right).\left(\frac{I_H}{I_{Ar}-E_i}\right)^2.\left[1+\frac{I_{Ar}-E_i}{5.I_H}.\left(1-3.l_i.(l_i+1)\right)\right] \qquad (4)$$

where I_H and I_{Ar} are the ionization potentials of hydrogen and argon atoms, E_i is the energy of the upper or lower state of argon to which the observed transition belongs and l_i is the orbital angular momentum of the optical electron of the state.

The active electron of the upper state of 772.38 nm Ar($1s_5$-$2p_7$) line is in *p* orbital, thus l_u=1 and in the lower state the electron is in *s* orbital, with l_l=0. In equation (4), replacing energies by their respective values[45] one can deduce R_u^2=55 and R_l^2=33.1, which finally lead to C_{6u}-C_{6l}=3.52x 10^{-32}. These values introduced in Eq. (3) provide $\Delta\lambda_{vdW}$=25.8 pm at 1 bar and 300 K for the 772.38 nm line.

For 772.42 nm Ar($1s_3$-$2p_2$) line, the orbital angular momentum of active electrons are again l_u=1 and l_l=0, resulting in R_u^2=64.2 and R_l^2=30.1, which lead to C_{6u}-C_{6l}=5.48x 10^{-32}, resulting finally in $\Delta\lambda_{vdW}$=31.0 pm at 1 bar and 300 K for this line.

If instead of using equation (3) recommended by Physicist's Desk Reference52 and by NIST[54], we start from the quantum-mechanical theory of hard sphere collisions, developed by Cowley[55] and described in Ref. 25, we can write:

$$\frac{\Delta\lambda_{vdW}}{[Ar]} = \frac{\lambda^2}{c}.\frac{4\pi}{3}.\left[\alpha_p.\frac{e^2.a_0^2}{h}.(R_u^2 - R_l^2)\right]^{2/5}.\langle v^{3/5}\rangle \qquad (5)$$

in which a_0 is the Bohr radius and $\langle v^{3/5}\rangle$ is defined as:

$$\langle v^{3/5}\rangle = 4\pi.\left[\frac{\mu}{2\pi RT_g}\right]^{3/2}.\int_0^\infty v^{2.6}.exp\left(-\frac{\mu.v^2}{2RT_g}\right).dv = \left(\frac{4}{\pi}\right)^{\frac{1}{5}}.\Gamma(1.8).\left(\frac{8RT_g}{\pi\mu}\right)^{3/10} \qquad (6)$$

where *v* corresponds to the mean relative velocity and R = 8.314 J/(mol.K). Corrected for the $(4/\pi)^{1/5}.\Gamma(1.8)$=0.9775 factor, this leads to relation (7), in which the factor 3.0 in equation (3) becomes 3.41:

$$\frac{\Delta\lambda_{vdW}}{[Ar]} = 3.41\,x10^{-15}.\lambda^2.(C_{6u} - C_{6l})^{2/5}.(T_g/\mu)^{3/10} \qquad (7)$$

Using this equation, the theoretical van der Walls broadening coefficients of 772.38 and 772.42 nm lines become 29.4 and 35.2 pm, respectively. These values will be compared to experimental data in section 6.1.

5. Absolute densities of Ar*($1s_5$) and Ar*($1s_3$) metastables

Integrating the absorbance in equation (1) over λ leads to:

$$\int_0^{\infty} \mathcal{A}_n(\lambda_n, t).d\lambda = \left(k_5.N_5(t) + k_3.N_3(t)\right).L \quad (8)$$

As shown in figures 3 and 6, and discussed in *section* 3, the absorbance curves can be fitted with two Voigt profiles $V_5(\lambda)$ and $V_3(\lambda)$, whose integrals are linked to the densities of Ar*($1s_5$) and Ar*($1s_3$) atoms, respectively. Reporting in (2) the transition probabilities of the lines: $A_{772.38}$=5.18 x10^6 s^{-1} and $A_{772.42}$=1.17 x10^7 s^{-1}, taken from 45, the calculated values of absorption coefficients, are k_5=1.47 x10^{-28} m^3 and k_3=1.66 x10^{-27} m^3. With L=0.05 m and the integrals of $V_5(\lambda)$ and $V_3(\lambda)$, coming from the fit of the absorbance curve, the deduced peak densities decrease from N_5=3.8 x10^{17} m^{-3} and N_3=7.5 x10^{16} m^{-3} at 312 mbar to N_5=1.2 x10^{17} m^{-3} and N_3=3.8 x10^{16} m^{-3} at atmospheric pressure. As was pointed out in *section 4*, the laser position inside the gap and the amplitude of the HV were adjusted at each pressure to obtain the largest absorbance. Therefore, no significant conclusion can be deduced from the diminution of the peak metastable densities when increasing the pressure. However, we have also observed a monotonical decrease of the ratio of peak densities N_5/N_3 from 5.1 at 312 mbar to 3.3 at atmospheric pressure. This evolution could be assigned to the more efficient excimer formation reaction from Ar*($1s_5$) atoms than from Ar*($1s_3$) metastables. The reported rate coefficients for the corresponding 3- body reaction:

$$Ar* + Ar + Ar \rightarrow Ar_2^* + Ar \quad (9)$$

are 1.1±0.4 x10^{-44} m^6s^{-1} and 0.83±0.3 x10^{-44} m^6s^{-1} for Ar*($1s_5$) and Ar*($1s_3$) atoms, respectively[50]. Corresponding decay times of $1s_5$ ($1s_3$) metastable atoms by reaction (9) would be 0.16±0.06 µs (0.21±0.08 µs) and 1.67±0.6 µs (2.2±0.8 µs) at 1000 and 312 mbar, respectively. However, the recorded time variation of metastable atom densities after the discharge breakdown, shown in figure 8, does not seem to confirm this prediction. First, as expected, the metastable atoms densities decay exponentially after the peak of the discharge current. But the measured decay time of about 1.15 µs at 312 mbar is shorter than the calculated 1.7 µs with the rate coefficient of ref 50. At the opposite, the decay times measured at 1 atmosphere: ≈1 µs for Ar*($1s_5$) atoms and 0.7 µs for Ar*($1s_3$) atoms, are much larger than the calculated ≈0.2 µs decay time. Also, a secondary peak of metastable density is clearly

visible in 816 mbar plasma and one observe an apparent production of excited atoms after the end of their initial fast decay at t≥4 µs, at 1 bar.

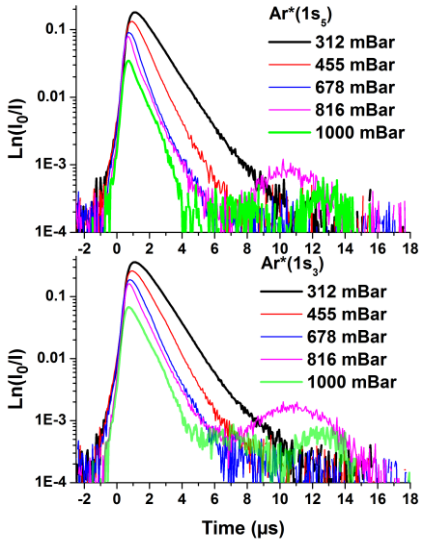

Figure 8. Time variation of absorbances (∝ to metastable densities) at different argon pressure. The time origin is the start of the fast discharge current increase at the positive half-period of the HV (for Ar(1s$_5$) atoms) and at the negative half-period of the HV (for Ar*(1s$_3$) atoms).*

More, a comparison of the time evolutions of the discharge current (Fig. 4) and Ar* densities (Fig. 8), indicates that the enhancement of the metastable atoms density starts before the discharge current pulse. In Fig. 8, we also note the presence of these phenomena on both densities of Ar*(1s$_5$) atoms, which are recorded at the positive half-period of the high voltage and those of Ar*(1s$_3$) atoms, which are recorded at the negative half-period of the HV. All these observations, suggest a small, but undeniable production of Ar* atoms outside the discharge current pulses. This production should thus be related to the heating of plasma electrons, before and after the discharge breakdowns, by the weak electric field present in the DBD gap. A detailed analysis of these observations will be presented in section 6.3 after the discussion on the line profiles and the relative density of the two metastable species.

6. Discussion

6.1. On 772.38 and 772.42 nm line profiles

To our knowledge, there are only few works in which the pressure broadening of 772 nm argon lines has been studied, or when these lines have been used for the plasma diagnostic. Penache *et al*, who had the appropriate diode laser to access these lines, reported in their publication on characterization of high pressure microdischarges[56]: "*The analysis of the transition at 772 nm could not be pursued, since the collision broadening parameters were not found in the literature.*". In a pulsed low pressure argon helicon plasma, Clarenbach *et al* have deduced the time variation of Ar*($1s_3$) metastable atoms by using laser absorption spectroscopy on 772.42 nm line and have deduced the gas temperature from the spectral profile of the absorption line[57]. We are aware of only two works reporting on characterization of 772 nm line profiles at high pressure. Moussounda and Ranson[28] have only measured the shift of the peak intensity of the lines emitted from a surfatron produced thermal plasma, with estimated gas temperature of 2000 K. Their reported shift values, corrected for the $T_g^{-0.7}$ gas temperature dependence, would correspond to 13.5±0.7 pm and 14.5±0.7 pm at 1 bar and 300 K for 772.38 and 772.42 nm lines, respectively. The about 10% larger values of these authors, compared to ours, can probably be linked to an underestimation of the gas temperature in their spatially inhomogeneous thermal plasma. Williamson *et al* measured the density of Ar*($1s_3$) metastable atoms in a DBD plasma by laser absorption spectroscopy on 772.42 nm line[58]. The spectral profile of the line has been recorded at different gas pressures, showing the line broadening with increased pressure. But they didn't provide a broadening coefficient. This probably was due to the large uncertainty they have encountered on determination of the gas temperature from the rotational temperature of N_2 emissions. However, an estimated value can be driven from the 2.1 GHz Lorentzian width, reported in Fig. 3 of their publication[58] for the highest studied pressure of 100 Torr, at 30 kHz pulse repetition rate and the gas temperature of T_g=410 K, indicated in their Fig. 5 for the considered conditions. Corrected for the pressure and T_g dependences, we find a pressure broadening coefficient of 19.9 GHz at 1 bar and 300 K. Considering the uncertainty linked to the gas temperature determination, this value, which corresponds to 40 pm, is in relatively good agreement with the 36.3 pm broadening coefficient of the 772.42 nm we have found for the standard conditions.

Table 1 summarize our measured data, the model calculated values and the other published values of our knowledge. Note the larger uncertainties on experimental values

relative to the 772.38 nm line, which, due to its weaker absorbance, has its profile partly affected by the wing of the 772.42 nm line profile. The measured ratios of shift/width are comparable to the values reported for argon lines[28, 29], or predicted for the Van der Waals interaction, with Lennard-Jones type potential[59]. The van der Waals widths calculated with equation (7) seems to be closer to our measured values rather than those deduced using equation (3), yet recommended in 52 and by NIST[54].

However, this better agreement can be purely fortuitous. Indeed, a realistic calculation of the van der Waals broadening must take into account the real molecular potentials of the interacting atoms, forming Ar*-Ar dimer. Ab-initio calculations on potentials of Ar_2^* molecule have been carried out by several groups[60, 61, 62]. But, to our knowledge, that potentials have never been used for deducing the pressure broadening constants of argon lines. The reason could be the lack of precision on calculated potentials. As an example, in 60, the calculated 0_u^+ and 1_u potential curves of Ar_2* dimer predict an energy difference of 0.00285 Hartree (625 cm^{-1}) between them at large atom separation. This should correspond to the energy gap between metastable Ar*($1s_5$) and resonance Ar*($1s_4$) states, which is exactly 607 cm^{-1}, as given by NIST[45]. More, authors of 61 indicate that their calculation predicts the atomic energy levels within 350 cm^{-1} of the experimental values.

Line	Width (Exp)	Shift (Exp)	Shift/Width	Width (Eq. 3)	Width (Eq. 7)	Width (Ref. 58)	Shift (Ref. 28)
772.38	28.3±2.0	11.5±0.8	0.4	25.8	29.4		13.5
772.42	36.3±0.5	12.8±0.7	0.35	31.0	35.2	40	14.5

Table1. Measured and calculated values (using equations (3) or (7)) of the pressure width (FWHM) and shift of the lines. All values are in pm, at atmospheric argon pressure and 300 K.

6.2. On relative peak densities of metastable atoms

In low pressure plasmas, the measured [Ar($1s_3$)]/[Ar($1s_5$)] density ratio was usually closer to 0.1 [63, 64, 65, 66], rather than to the statistical value $(2J_3+1)/(2J_5+1)=0.2$, where $J_3=0$ and $J_5=2$ are the total angular momentum of $1s_3$ and $1s_5$ sates, respectively. The observed enhancement of this ratio with increasing argon pressure, reaching 0.3 at atmospheric pressure, can be related to both smaller reaction coefficient of Ar*($1s_3$) atoms in 3-body collision with 2 Ar atoms (Eq. 9) (longer lifetime for these atoms)[50], or to a more efficient production rate of these atoms by collisional transfers from the resonance state Ar($1s_2$), involving Ar atoms and/or bulk electrons. In fact, the cross-section for electron impact excitation of argon into $1s_3$ metastable state is about 1 x 10^{-22} m^2, compared to 2 x 10^{-21} m^2 for

the resonance $1s_2$ state and 1 x 10^{-21} m^2 for both $1s_4$ and $1s_5$ states[67]. Thus, e-impact excitation of Ar atoms should strongly overpopulate $1s_2$ state relative to $1s_3$. Reported quenching rate coefficients of argon metastable atoms colliding with ground state Ar atoms are[50]: k_5=2.1 x 10^{-21} m^3s^{-1} and k_3=5.3 x 10^{-21} m^3s^{-1}. From the study of Ar collision induced transfers within excited Ar*(2p) and Ar*(3p) states, it was found that transfers with the inner ion core conservation of the excited atom are highly favored[68, 69]. As indicated in Table II of 68, collisional transfers within the group of 4 levels $2p_1$, $2p_2$, $2p_3$ and $2p_4$, which have ion core configuration $Ar^+(^2P_{1/2})$ and within the group of 6 levels $2p_5$ to $2p_{10}$, having $Ar^+(^2P_{3/2})$ as ion core[45], are much favored compared to inter-group transfers. Regarding 1s states, $1s_2$ and $1s_3$ have $Ar^+(^2P_{1/2})$ ion core and $1s_4$ and $1s_5$ have $Ar^+(^2P_{3/2})$ ion core. Thus, considering the closeness of the states, it can be assumed that $k_3 \approx k_{32}$ transfer rate coefficient to $1s_2$ and $k_5 \approx k_{54}$, transfer to $1s_4$ state. Given that the reverse transfer rate coefficients are linked to the direct transfers by the detailed balancing principle: $(k_{ij}/k_{ji})=(2J_j+1)/(2J_i+1)$ x Exp(-ΔE/kT), where ΔE is the energy gap between levels, the room temperature value of the transfer coefficient from $1s_2$ to $1s_3$ can be deduced as[63] k_{23}=22 x 5.3 x $10^{-21} \approx 1.2\ 10^{-19}$ m^3s^{-1} and k_{45}=31 x 2.1 x $10^{-21} \approx 6.5\ 10^{-20}$ m^3s^{-1}. This Ar-induced transfer of population to $1s_3$ state would correspond to a decay frequency of $1s_2$ population density of about 1 and 3 x 10^6 s^{-1} at 0.321 and 1 bar, respectively. This frequency is comparable to the loss frequency of $1s_2$ atoms by 3-body reaction forming Ar_2* excimer (Reaction 9). In conclusion, at high pressure plasmas, large amount of atoms in the highly over-populated Ar*($1s_2$) resonance state will be collisionally transferred to its neighboring Ar*($1s_3$) metastable state, whose direct excitation from the ground state is inefficient. But for the $1s_4$-$1s_5$ coupled states, first the k_{45} transfer rate is 3 times smaller than k_{23}; and second, the e-impact production rates of $1s_4$ and $1s_5$ states are comparable, thus the $1s_4 \rightarrow 1s_5$ transfers contribution to the net Ar*($1s_5$) metastable density is much less important.

Besides Ar-induced transfers, e-impact induced transfers can also contribute to the indirect population of metastable states. Rate coefficients in the range of a few times 10^{-13} m^3s^{-1} have been reported for the e-induced population transfers between resonance and metastable states of Ar(1s) group[70, 71]. With an electron density of a few times 10^{18} m^{-3}, the transfer rates will also be in the range of 10^6 s^{-1}. However, during the discharge pulse, when T_e is larger than the fraction of eV, thus of the energy separation between Ar(1s) states, these transfers should tend to establish a statistical population distribution between the 4 Ar(1s)

states. But in the absence of an important inter-gap E-field, the room temperature bulk electrons should preferentially induce down-ward transfers toward metastable states.

6.3. On time evolution of Ar*(1s) density

As pointed out before, the analysis of the kinetic of Ar* metastable atoms reveals the presence of a weak production channel for them prior and after the breakdown of the intense discharge current pulse. This channel can be linked to the secondary photoelectron generation from the instantaneous cathode of the DBD by VUV photons emitted from argon excimers Ar_2^* formed by reaction (9)[44]. Accelerated by the E-field present in the gas gap, these electrons can maintain a discharge current and induce excitation and ionization of ground state Ar atoms. To illustrate this assertion, the time variation of the absorbance when the laser wavelength is set at the maximum absorbance of the 772.42 nm line (corresponding to the maximum density of Ar*($1s_3$) atoms) is shown in figure 9 for argon pressure of 816 mbar, together with the corresponding discharge current, applied high voltages (V_a) and the calculated voltage seen by the gas inside the gap, V_g.

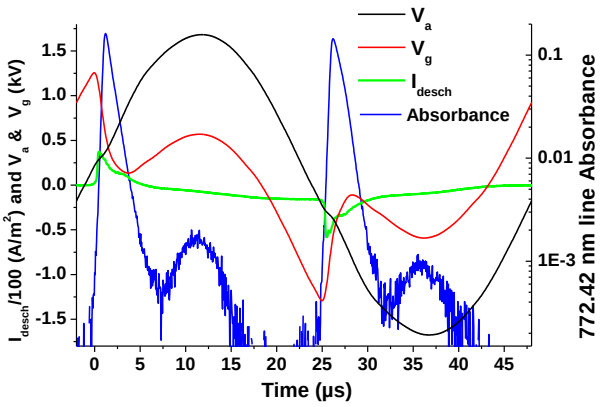

Figure 9. Time variation of applied voltage V_a (black), the voltage V_g seen by the gas gap (red), discharge current (green), and the absorbance when the laser is set at the maximum absorption by Ar($1s_3$) metastable atoms (blue) at 816 mbar argon pressure. The time origin is the start of the fast increase of the discharge current at the positive half-period of the HV. Note the logarithmic scale for the 772.42 nm line absorbance.*

A perfect correlation in time is observed between the 2nd maximum of V_g and the second maximum of Ar* metastable density. As the phenomena are identical on positive and negative half-cycle, we only analyze the first half-cycle, when HV is positive. In Figure 9,

discharge breakdown occurs at t≈0 µs, when V_g reaches $V_{g\text{-}b}$=1250 V. After breakdown, the peak current density reaches a value about 40 A/m^2 and then decreases slowly. Drift of charges, generated by the ionization of the gas, toward electrodes and their accumulation on the internal surfaces of the dielectrics progressively screens the externally applied voltage, inducing the drop of V_g down to a minimum value of $V_{g\text{-}m}$=135 V at t_m≈3.7 µs. Beyond, with increasing amplitude of V_a, the applied HV, the amplitude of V_g increases again up to a secondary maximum of $V_{g\text{-}s}$≈570 V, reached at the same time t_s≈12 µs than the maximum of V_a. With these values of V_g, the gas pressure 816 mbar and 310 K gas temperature, the calculated reduced electric field $F=E/N$ acting on the gas are F_b=33 Td, F_m=3.5 Td and F_s=15 Td respectively at the breakdown, at the minimum of V_g and at the secondary maximum of V_g.

As seen in figure 9, the peak of Ar*(1s$_3$) metastable density occurs at t_p≈1.5 µs after the discharge breakdown. Given the about 250 ns lifetime of Ar* atoms at 816 mbar, their density evolution mostly reflects the time variation of their production rate. Thus the observed 1.5 µs delay indicates that from the breakdown up to the Ar(1s) peak density, their production rate largely overpasses their loss rate. At t_p=1.5 µs, the discharge current has still 70% of its peak value and V_g has dropped from 1250 V to 570 V. In this range, the voltage seen by the gas gap remains high enough to maintain an efficient production of metastable atoms. But after the Ar*(1s) peak, its loss by 3-body reaction (9) overpasses its e-impact excitation from the ground state Ar atoms. The rate coefficient for excitation to Ar*(1s) states, calculated with Bolsig+ code[72] (Version 12/2017 with Biagi data set) by using the reduced field at the maximum of Ar(1s) peak, is k_e≈ 1.5 x 10^{-17} m^{3}s^{-1} for V_g=570 V. This is only 4 times smaller than the k_e value calculated for $V_{g\text{-}b}$=1250 V at the breakdown while k_e drops to 1.2 x 10^{-20} m^{3}s^{-1} for the minimum value of V_g, $V_{g\text{-}m}$=135 V, reached at t_m≈3.7 µs. At this time, the density of atoms in Ar*(1s) states reaches its minimum, which is about 3 orders of magnitude smaller than its peak value. After t_m, both V_g, and Ar*(1s) density again increase, reaching their respective maximum value at t_s≈12 µs. At this secondary maximum, where the reduced electric field becomes again F_s=15 Td, the excitation rate coefficient is increased by 3 orders of magnitude to reach k_e≈ 1.5 x 10^{-17} m^{3}s^{-1}. We are aware that the amount of Ar*(1s) atoms produced by e-impact from the ground state to balance their loss by 3-body reaction of Eq. (9) depends also on electron density, which is largely smaller at t_s≈12 µs than at t_p≈1.5 µs. This is the reason why for the same V_g=570 V, thus similar k_e≈1.5 x 10^{-17} m^{3}s^{-1}, the Ar*(1s) atoms

density is almost 2 orders of magnitude smaller at $t_s \approx 12$ µs than at $t_p \approx 1.5$ µs. This is also the explanation of the non-measurable Ar(1s) density when the voltage amplitude increases in the following half cycle as the electrons trapped in the positive column are drifted to the anode when the V_g polarity is reversed.

In conclusion, argon atoms in metastable states can be produced outside the discharge current pulse which follows the breakdown. The electric field, resulting from the externally applied voltage and charges accumulated in the internal surfaces of dielectrics during the discharge pulse, is high enough for heating electrons, giving them a mean energy of a few eV. This E-field, whose amplitude is well below the necessary E-field to induce a breakdown, is, however, high enough for maintaining a weak excitation in the gas. Nevertheless, looking on figure 8, a question arises: why a distinctly observed secondary maximum on Ar* metastable density is only present at 816 mbar argon pressure? This peculiarity can be attributed to the more significant enhancement at this pressure of V_g, then of the *E/N* in the gas gap, between their minimum values $V_{g\text{-}m}$ and their secondary maxima, $V_{g\text{-}s}$. To illustrate the point, values of $V_{g\text{-}m}$ and $V_{g\text{-}s}$ on the five studied gas pressures are reported in Table 2, together with reduced field values corresponding to them. We note that the most significant enhancement on *E/N* between the minimum and the secondary maximum of V_g occurs in 816 mbar plasma. Also, in 1 bar plasma, *E/N* remains moderately high, evolving from 6 to 13 Td between these two positions. As a consequence, in this plasma, a weak production channel of Ar* atoms maintains their density to none zero value during that period. As was pointed out before, for each pressure, the amplitude of the applied HV was adjusted for obtaining stable and reproducible discharges, but at the lowest possible voltage to limit the electron density. Thus at this state, it is not possible to analyze the influence on $V_{g\text{-}m}$ and $V_{g\text{-}s}$ of the applied HV amplitude, $V_{a\text{-}m}$. A systematic study of the time evolution of Ar* atoms density and of V_g when varying the amplitude of the HV, would certainly help for getting a better insight on physical processes responsible for the production of Ar* metastable atoms outside the discharge current pulse initiated by the breakdown.

.

Pressure (mbar)	312	455	678	816	1000
$V_{a\text{-}m}$ (V)	795	950	1350	1680	1780
$V_{g\text{-}m}$ (V)	97	50	106	136	300
$V_{g\text{-}s}$ (V)	120	134	320	570	645
E/N_m (Td)	6.5	2.5	3.3	3.5	6
E/N_s (Td)	8	6	10	15	13

Table2. Amplitude of the applied voltage ($V_{a\text{-}m}$) and the voltage in the gas gap at its minimum ($V_{g\text{-}m}$) and secondary maximum ($V_{g\text{-}s}$) at studied gas pressures. *E/N* values corresponding to $V_{g\text{-}m}$ and $V_{g\text{-}s}$ are also given. Uncertainties on reported *V* and *E/N* values are less than 10%.

7. Acknowledgments

The work was supported by the Agence Nationale de la Recherche through the Investissement d'avenir program (ANR10LABX2201). The "Réseau des Plasmas Froids" of CNRS/MRCT (France) is acknowledged for providing the DFB diode laser and the travel support for Nader Sadeghi. The authors thanks Gerjan Hagelaar for his advices in using Bolsig+ code and Serge Béguier for his contribution to the double Voigt fit of profiles.

References

[1] Z. Chen, X. Cheng, L. Li and M. Keidar, J. Phys. D: Appl. Phys. **50** (2017) 015208
[2] K. Shimizu, N. A. Tran, K. Hayashida and B. Blajan, J. Phys. D: Appl. Phys. **49** (2016) 315201
[3] H.A. Aboubakr, U. Gangal, M.M. Youssef, S.A. Goyal and P.J. Bruggeman, J. Phys. D: Appl. Phys. **49** (2016) 204001.
[4] N. Barekzi and M. Laroussi, Transactions on Plasma Science **42** (2014) 2738
[5] B.K.H.L. Boekeman *et al*, J. Phys. D: Appl. Phys. **48** (2016) 044001
[6] M. Engelhardt, K. Kartaschew, N. Bibinov, M. Havenith and P. Awakowicz, J. Phys. D: Appl. Phys. **50** (2017) 015206
[7] X. Lu, G.V. Naidis, M. Laroussi, S. Reuter, D.B. Graves and K. Ostrikov, Physics Reports **630** (2016) 1
[8] J. Winter, R. Brandenburg and K-D. Weltmann, Plasma Source Sci. Technol, **24** (2015) 064001
[9] R. Brandenburg, Plasma Source Sci. Technol, **26** (2017) 053001
[10] P.J. Bruggeman *et al*, Plasma Source Sci. Technol, **25** (2015) 053002
[11] D.B. Graves, Physics of Plasmas, **21** (2014) 080901
[12] F. Massines, P. Segur, N. Gherardi, C. Khamphan and A. Ricard, Surf. Coat. Technol. **174** (2003) 8
[13] D.X. Liu, P. Bruggeman, F. Iza, M.Z. Rong and M.G. Kong, Plasma Source Sci. Technol, **19** (2010) 025018
[14] K. Niemi, J. Waskoenig, N. Sadeghi, T. Gans and D. O'Connell, Plasma Source Sci. Technol, **20** (2011) 055005
[15] S.A. Norberg, E. Johnsen and M.J. Kushner, Plasma Source Sci. Technol, **24** (2015) 035026.
[16] T. Verreycken, R.M. van der Horst, N. Sadeghi and P. Bruggeman, J. Phys. D: Appl. Phys. **46** (2013) 464004
[17] P.J. Bruggeman, N. Sadeghi, D.C. Schram and V. Linss, Plasma Source Sci. Technol, **23** (2014) 023001
[18] P.J. Bruggeman, G. Cunge and N. Sadeghi, Plasma Source Sci. Technol, **21** (2012) 035019
[19] G. Cunge, R. Ramos, D. Vempaire, M. Touzeau, M. Nejbauer and N. Sadeghi, J. Vac. Sci. Technol. **A 27** (2009) 471
[20] A. Rousseau, E. Teboul and N. Sadeghi, Plasma Source Sci. Technol, **13** (2004) 166
[21] S. Hübner, N. Sadeghi, E.A.D. Carbone and J.J.A.M. van der Mullen, J. Appl. Phys. **113** (2013) 143306
[22] N. Allard and J. Kielkopf, Rev. Mod. Phys. **54**, (1982) 1103
[23] A. Durocher-Jean, E. Desjardins, and L. Stafford 2019, Phys. Plasmas **26**, 063516
[24] D. M. Camm and F. L. Curzon, 1972 Can. J. Phys. **50**, 2866
[25] C. Lee, D M. Camm and G H. Copley 1975 *J. Quantitative Spectroscopy and Radiative Transfer* **15** 211
[26] W. R. HindmarshI and K. A. Thomas, 1961 Proc.phys. Soc. **A77**, 1193
[27] Stacey D and Vaughan J 1964 *Physics Letters* **11** 105
[28] P S. Moussounda and P. Ranson 1987 J. Phys. B: At. Mol. Phys. **20,** 949
[29] G H. Copley and D M. Camm, 1974 *J. Quantitative Spectroscopy and Radiative Transfer* **14** 899
[30] G H. Copley 1976 *J. Quantitative Spectroscopy and Radiative Transfer* **16** 377
[31] G H. Copley 1976 *J. Quantitative Spectroscopy and Radiative Transfer* **16** 553
[32] O. Vallee, P. Ranson and J. Chapelle 1977 *J. Quantitative Spectroscopy and Radiative Transfer* **17** 327
[33] we use Paschen notation for the identification of excited states and transitions. $1s_3$ and $1s_5$ metastable states are identified as $^3P_0$ and $^3P_2$ in L-S coupling and $4s'[1/2]_0$ and $4s[3/2]_2$ in Rackah notation.
[34] K Tachibana, H Harima and Y Urano 1982, J. Phys. B: At. Mol. Phys. **15** 3169
[35] B. Niermann, M. Boke, N. Sadeghi, and J. Winter, 2010 Eur. Phys. J. D 60 , 489
[36] P A. Mikheyev, A K. Chernyshov, N I. Ufimtsev, E A. Vorontsova, V N. Azyazov 2015, *J. Quantitative Spectroscopy and Radiative Transfer* **164** 1
[37] A. V. Pipa, Yu. Z. Ionikh, V. M. Chekishev, M. D€unnbier, and S. Reuter 2015 Appl. Phys. Lett. **106** 244104
[38] A. Schmidt-Bleker, J. Winter, A. Bosel, S. Reuter and K-D Weltmann 2016 Plasma Source Sci. Technol, **25** 015005
[39] B. Eshel, Ch A. Rice, G P. Perram 2016 *J. Quantitative Spectroscopy and Radiative Transfer* **179** 40
[40] A.K. Chernyshov, P.A. Mikheyev, N.I. Ufimtsev 2019 *J. Quantitative Spectroscopy and Radiative Transfer* **222** 84
[41] G. Nayak, M-S Simeni, J. Rosato, N. Sadeghi, and P. J. Bruggeman 2020 J. Appl. Phys. **128**, 243302
[42] F. Massines, N. Gherardi, N. Naude and P. SegurRecent 2009, Eur. Phys. J. Appl. Phys. **47**, 22805
[43] N. Naudé, J.P. Cambronne, N. Gherardi, F. Massines, 2005, Eur. Phys. J. Appl. Phys. **29**, 173
[44] R. Robert, G. Hagelaar, N. Sadeghi, R. Magnan, L. Stafford, F. Massines, *To be published*
[45] NIST Atomic Spectra Database: https://physics.nist.gov/asd
[46] G. Cunge, R. Ramos, D. Vempaire, M. Touzeau, M. Neijbauer, and N. Sadeghi, 2009 J. Vac. Sci. Technol. A **27**, 471
[47] S G. Belostotskiy, V M. Donnelly, D J. Economou, and N. Sadeghi, 2009 IEEE Trans. Plasma Sci., **37**, 852
[48] J Winter, J Santos Sousa, N Sadeghi, A Schmidt-Bleker, S Reuter and V Puech 2015, PSST **24**, 025015

[49] N. Sadeghi 2004, J. Plasma Fusion Res. **80**, 767
[50] Kolts J H and Setser D W 1978, J. Chem. Phys. **68,** 4848
[51] N. Konjevic, A. Lesage, J. R. Fuhr and W. L. Wiese 2002, J. Phys. Chem. Ref. Data, **31**, 819
[52] A Physicist's Desk Reference, AIP 1989, ISBN 0-88318-629-2, page 101
[53] J. Mitroy, M S. Safronova and C W. Clark 2010, J. Phys. B: At. Mol. Opt. Phys. **43** 202001
[54] https://www.nist.gov/pml/atomic-spectroscopy-compendium-basic-ideas-notation-data-and- formulas/atomic-spectroscopy-6
[55] C R. Cowley, 1970, The Theory of Stellar Spectra, p. 200 Gordon & Breach, New York
[56] C. Penache, M. Miclea, A. Brauning-Demian, O. Hohn, S. Schossler, T. Jahnke, K. Niemax and H. Schmidt-Bocking 2002, PSST **11**, 476
[57] B Clarenbach, B Lorenz, M Kramer and N Sadeghi 2003, PSST **12**, 345
[58] J M. Williamson, P. Bletzinger and B N. Ganguly 2004, J. Phys. B: At. Mol. Phys. **37,** 1658
[59] H M. Foley 1946, Phys. Rev. **69**, 616
[60] C. Teichteil and F. Spiegelmann 1983, Chemical Physics **81,** 383
[61] F. Spiegelmann and F X. Gadea 1984, J. de Physique **45,** 1003
[62] M. Selg 2008, Phys. Scr. **77** 015302
[63] E. Ellis and N D. Twiddy, 1969, , J. Phys. B: At. Mol. Phys. **2,** 1366
[64] N. Sadeghi, M. Cheaib and D W. Setser 1989, J. Chem. Phys. **90,** 219
[65] T D. Nguyen and N. Sadeghi 1983, Chemical Physics **79,** 41
[66] B. Bakowski, G. Hancock, R. Peverall, S E. Prince, G A D. Ritchie and L J. Thornton 2005, J. Phys. D: Appl. Phys. **38**, 2769
[67] M A. Khakoo *et al* 2004, J. Phys. B: At. Mol. Phys. **37,** 247 and M A. Khakoo, O. Zatsarinny and K. Bartschdat 2011, J. Phys. B: At. Mol. Phys. **44,** 015201
[68] T D. Nguyen and N. Sadeghi 1978, Phys. Rev. A **18**, 1388
[69] G. Inoue, D W. Setser and N. Sadeghi 1982, J. Chem. Phys. **76,** 977
[70] E A D. Carbone, S. Hubner, J J A M. van der Mullen, G M W. Kroesen and N. Sadeghi 2013, J. Phys. D: Appl. Phys. **46**, 415202
[71] E. Carbon, E. van Veldhuizen, G. Kroesen and N. Sadeghi 2015, J. Phys. D: Appl. Phys. **48**, 425201
[72] G J M. Hagelaar and L C. Pitchford 2005 *Plasma Sources Sci. Technol.* **14** 722